Two observable features of the staggered-flux phase at nonzero doping

T. C. Hsu
Department of Physics, University of British Columbia, 6224 Agriculture Road, Vancouver, British Columbia, Canada V6T-2A6

J. B. Marston
Laboratory of Atomic and Solid State Physics, Cornell University, Ithaca, New York 14853-2501

I. Affleck
Department of Physics, University of British Columbia, 6224 Agriculture Road, Vancouver, British Columbia, Canada V6T-2A6
(Received 15 August 1990)

We investigate whether the staggered-flux phase (SFP) is realized in slightly doped phases of the Cu-O high-T_c superconductors. Using a mean-field solution of the t-J model, we calculate the size of circulating currents in the CuO_2 planes. For realistic parameters we find nonzero currents when the doping $\delta < 0.12$. Taking into account structural details, we calculate the physical magnetic-field strength and the neutron-scattering cross section. The static field at the muon site varies between 0 and 100 G depending mainly on doping but with additional complications being the size of the Wannier functions, temperature, screening, localization, and the mean-field-approximation itself. These fields are not detected in muon-spin-relaxation experiments but cannot be ruled out both because of the aforementioned complications and because at low doping the muon is also affected by residual quasistatic spin moments. Neutrons scattering off orbital moments of the SFP exhibit a Bragg peak at wave vector $(\pi/a,\pi/a)$ even at nonzero doping; however, this peak is perhaps 70 times weaker than that produced by static spin moments in a fully Néel ordered phase and is therefore difficult to observe. The absence of quasistatic spin moments in our description conflicts with neutron experiments on lightly doped samples. The inelastic spin structure does, however, exhibit a split peak at wave vector $(\pi/a,\pi/a)$ in qualitative agreement with neutron experiments on superconducting $La_{2-x}Sr_xCuO_4$ samples but additional structure along the $(Q_x,0)$ and $(0,Q_y)$ directions has not been seen. The absence of magnetic fields when $\delta > 0.12$ is consistent with the limits set by the muon experiments on superconducting samples. We show that similar results are obtained using the Gutzwiller-projected SFP.

I. INTRODUCTION

The two-dimensional one-band large-U Hubbard model near half-filling has been subject to intense scrutiny during the past three years since it seems to be a reasonable model of copper oxide superconductors.[1] In two mean-field treatments of this model, a special saddle point was discovered by Kotliar[2] and independently by Affleck and Marston,[3,4] who called it the "flux phase." The orbital motions of electrons in this state are identical to those of charges in tight-binding model with a spatially alternating external magnetic flux threading through adjacent plaquettes of the square lattice. The removal of the doubly occupied subspace can be enforced by Gutzwiller projection and, at half-filling, the resulting state, viewed as a variational wave function, has a fairly good energy.[5–10] The doped staggered-flux phase (SFP) with Cooper pairing was recently proposed by Zhang[6] and Wang, Kotliar, and Wang[11] to describe the superconducting ground state.

Some observable properties, in the normal state, of the doped staggered-flux phase include muon spin rotation (μSR) in the physical magnetic fields due to circulating electronic currents and neutron scattering off these orbital moments as well as off the electron spins. One advantage of focusing on these local probes as opposed to transport and optical properties, for example, is that local probes are less sensitive to complications like impurities, surface contamination, and grain boundaries. We calculate the behavior of these two features and compare them with experiment.

It is important to note that muons and neutrons are sensitive to fluctuations in the magnetic fields at different time scales. Neutron experiments typically examine energy transfers greater than 1 meV; neutrons, therefore, can detect fluctuations with frequencies greater than 10^{12} Hz. Muons, on the other hand, are sensitive to magnetic fields fluctuating no faster than 10^{11} Hz for field strength amplitudes of order 100G (this upper frequency bound is lower for weaker fields).[12] Of course, both probes respond to static fields, but the different frequency windows can be used to isolate distinct sources of fluctuating magnetic fields. Finally, the muon signal contains information about the degree of spatial randomness in the magnetic fields. It might be possible to use this information to separate the periodic orbital magnetic fields of the SFP from the disordered quasistatic spin moments known to be present in lightly doped high-T_c materials.

II. THE STAGGERED-FLUX PHASE

The Hamiltonian of the one-band repulsive Hubbard model with a nearest-neighbor hopping integral

$$t_{xy}=t\exp\frac{ie}{\hbar c}\int_x^y \mathbf{A}\cdot d\mathbf{l} \tag{1}$$

(where $\mathbf{A}$ is the Maxwell gauge field) may be written using the fermionic electron operators $c_{x\sigma}$ as

$$H=\sum_{\langle x,y\rangle} t_{xy}(c_x^{\dagger\sigma}c_{y\sigma}+\text{H.c.})+\sum_x Un_{x\uparrow}n_{x\downarrow}\ . \tag{2}$$

Here, and in the following equations, we define the electrons to carry the electric charge. The electrons are therefore responsible for any real magnetic fields that arise. (We could just as well have defined the holes to carry the charge. Our final results would be the same, however, since the assignment of charge is arbitrary.) The first sum is over nearest-neighbor copper-atom sites $\mathbf{x}$ and $\mathbf{y}$ and a sum over the spin index σ is implied. For large U/t (appropriate here), the dynamics of the low-energy subspace with no doubly occupied sites (p-type doping) is described by the t-J Hamiltonian with *chargeless* spinless bosonic holes (b_x operators):[13,14]

$$H=\sum_{\langle x,y\rangle} t_{xy}(b_y^{\dagger}b_x c_x^{\dagger\sigma}c_{y\sigma}+\text{H.c.})+J(\mathbf{S}_x\cdot\mathbf{S}_y-\tfrac{1}{4}n_x n_y)\ . \tag{3}$$

Here $J=4t^2/U$ is the magnetic exchange constant and $\mathbf{S}_x\equiv\frac{1}{2}c_x^{\dagger\alpha}\boldsymbol{\sigma}_\alpha^\beta c_{x\beta}$. To be definite we use the values $t=0.44$ eV obtained by Hybertsen *et al.*[15] and $J=0.13$ eV by Singh *et al.*[16] These values are not expected to vary by more than 10% among the different copper oxide materials.

A local constraint $c_x^{\dagger\sigma}c_{x\sigma}+b_x^{\dagger}b_x=1$ is imposed on the fermions and bosons to forbid double occupancy by either holes or electrons. [Only electrons appeared in the Hamiltonian of an earlier large-n analysis of a SU(n) t-J model.[3,4] The flux phase in that case exhibited physical currents even at zero doping because large, but finite, on-site repulsion U does not eliminate single-particle charge fluctuations in the large-n limit. In this paper we completely forbid double occupancy by introducing explicit hole fields and the currents disappear when no holes are present.] We drop the last term in Eq. (3) in the following analysis, since the phases we study in our mean-field approximation have uniform charge density. (In any case, phase separation into large hole-rich and hole-poor regions is forbidden by the long-range Coulomb forces.) The t-J model can now be transformed, using the functional integral approach, into a form suitable for our mean-field approximation by introducing complex bosonic Hubbard-Stratonovich fields χ_{xy} on the links of the lattice to factorize the four-fermion spin-spin interaction.[3,4] The resulting (imaginary time) Lagrangian may be written

$$L=\sum_x\{c_x^{\dagger\sigma}\partial_t c_{x\sigma}+b_x^{\dagger}\partial_t b_x-\mu[c_x^{\dagger\sigma}c_{x\sigma}-(1-\delta)]\}$$
$$+\sum_{\langle x,y\rangle}\{(2/J)|\chi_{xy}|^2$$
$$+[(t_{xy}b_y^{\dagger}b_x+\chi_{xy})c_x^{t\sigma}c_{y\sigma}+\text{H.c.}]\}\ . \tag{4}$$

Here μ is the chemical potential that must be adjusted to obtain the desired filling fraction $1-\delta$. Actually, an additional on-site term

$$i\sum_x\lambda_x(c_x^{\dagger\sigma}c_{x\sigma}+b_x^{\dagger}b_x-1)$$

appears in the Lagrangian to enforce the local occupancy constraint. Since λ_x is a constant at the flux saddle point and does not affect the single-particle states nor the total saddle-point energy, we will ignore it.

In this paper we take the link bosons to be static mean fields and study the saddle-point approximation [justified in the large-n limit of a SU(n) generalization of the model] described by $\chi_{xy}=|\chi|e^{i\theta'/4}$, where the links are oriented as shown in Fig. 1. The dependence of θ' on t/J and the doping δ is determined by minimizing the free energy (see below). Our staggered-flux phase naturally incorporates the "uniform" or Fermi-liquid phase for which $\theta'=0$. The hole bosons completely condense (at zero temperature) so we can set $b_x=\delta^{1/2}$. (The phases of the Bose fields can be absorbed into the fermions, so we may choose b_x to be purely real. The bosons condense into a zero-momentum state.) This saddle point is locally unstable at low doping towards a localized "box" phase with spin-Peierls enhancement on $\frac{1}{4}$ of the plaquettes;[17] however, the addition of a biquadratic spin-spin interaction stabilizes the SFP in the large-n limit without altering the

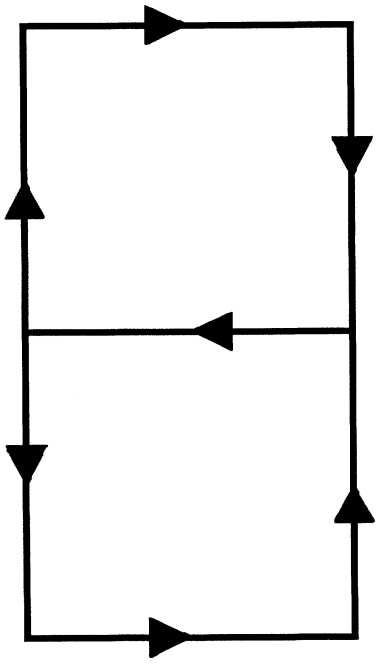

FIG. 1. The $\sqrt{2}$ unit cell: orientations of the complex χ_{xy} link fields (the currents flow in the same pattern).

physical SU(2) system.[2] (At $\frac{1}{4}$ filling, Sachdev[18] found that, in the absence of biquadratic coupling, a dimerized state is the global saddle point when $t/J<0.3$. Sufficient biquadratic coupling should eliminate this phase; in any case, the ratio t/J is too small to be relevant to the copper oxide systems. Also, the incommensurate flux instability reported in Ref. 11 occurs only over an extremely narrow range of doping $[0<\delta\lesssim 0.01(J/t)^2\sim 0.001]$ and we will ignore it.) Finally, the staggered flux phase is also stable against dimerization within the Gutzwiller-projection mean-field scheme[5,7-10] (see the Appendix). Henceforth, we assume that no spin-Peierls modulation develops.

Because the link fields can have an imaginary component, the electrons move through the lattice in our mean-field approximation as if they were tight-binding electrons hopping from site to site in a fictitious applied magnetic field. The unit cell contains just two (even and odd) sites because the fictitious field alternates in sign depending on whether the plaquette is centered on an even or odd dual lattice site. (In contrast to the anyon,[19] uniform-flux,[20] and commensurate-flux[21] theories, the staggered-flux phase does not break time-reversal symmetry globally because translation by one site combined with the time-reversal operation is a symmetry. Note that the commensurate- and uniform-flux phases have higher energies than the SFP.[20]) The single-particle wave functions are thus eigenstates of the hopping Hamiltonian:

$$H_{\rm sp}=\sum_{\langle x,y\rangle}[(t_{xy}\delta+\chi_{xy})c_x^{\dagger\sigma}c_{y\sigma}+\text{H.c.}]\ . \tag{5}$$

In addition to the staggered fictitious flux $\pm\theta'$ passing through the plaquettes, a real (Maxwell) magnetic flux (also staggered) Φ appears in the electronic hopping integral t_{xy} because, as we show below, real magnetic fields arise in the doped flux phase. So, $t_{xy}=te^{i\phi/4}$, where $\phi=e\Phi/hc$ and the t_{xy} are oriented in the same pattern as Fig. 1. The phases of the χ_{xy} fields are not modified by real magnetic fields, however, since the spin-spin interaction involves no charge currents.

As far as the set of single-particle electron eigenstates is concerned, only the combined flux (real and fictitious) acting on the electrons is important. We will therefore speak of an effective flux θ that characterizes these states. It is given by

$$\tan(\theta/4)=\frac{|\chi|\sin(\theta'/4)+t\delta\sin(\phi/4)}{|\chi|\cos(\theta'/4)+t\delta\cos(\phi/4)}\ . \tag{6}$$

The single-particle eigenstates break up into upper and lower bands:

$$H_{\rm sp}\psi_{\pm}^{\dagger}(\mathbf{k})|0\rangle=\pm\varepsilon(\mathbf{k})\psi_{\pm}^{\dagger}(\mathbf{k})|0\rangle\ , \tag{7}$$

with energies

$$\varepsilon(\mathbf{k})=2\bar{\chi}[\cos^2(k_xa)+\cos^2(k_ya)+2\cos(\theta/2)\cos(k_xa)\cos(k_ya)]^{1/2}\equiv 2\bar{\chi}\Gamma(\mathbf{k},\theta)\ , \tag{8}$$

where

$$\bar{\chi}^2=|\chi|^2+(t\delta)^2+2t\delta|\chi|\cos(\theta'/4-\phi/4)$$

and $a=3.8$ Å is the CuO_2 lattice constant. The eigenstates are a linear combination of the Fourier modes on the even and odd sublattices:

$$\psi_{\pm}^{\dagger}(\mathbf{k})=2^{-1/2}[c_e^{\dagger}(\mathbf{k})\pm g(\mathbf{k})c_o^{\dagger}(\mathbf{k})]\ , \tag{9}$$

where the phase factor $g(\mathbf{k})$ is given by

$$g(\mathbf{k})=\frac{e^{i\theta/4}\cos(k_xa)+e^{-i\theta/4}\cos(k_ya)}{|e^{i\theta/4}\cos(k_xa)+e^{-i\theta/4}\cos(k_ya)|}\ . \tag{10}$$

These electron eigenstates provide a convenient basis for the calculations that follow.

The energy density of the Maxwell flux generated by orbital currents is always insignificant and does not influence the saddle point. The maximum current that passes through a link is given by $2te/\hbar$. That value is for an electron with momentum $\hbar\pi/2a$. The typical magnetic field caused by such current is of order $te/\hbar ca$. It can be shown that the geometrical factor due to adding up the contribution from all the links on a lattice is at most of order 10. Typical energies per site are thus $a^3B^2\sim t(e^2/a)/m^*c^2$. Here $t\equiv\hbar^2/2m^*a^2$ and m^* is the noninteracting effective electron mass which takes the value $m^*/m=0.26\ \text{eV}/t$. So the importance of the magnetic-field energy is reduced by the ratio of a few eV divided by the electron rest mass energy. Likewise, the amount of *real* flux is reduced from $\phi_0=hc/e$ by the same factor. The flux ϕ appearing in Eq. (6) may therefore be set to zero for the purposes of our energy-optimization calculation. Nevertheless, note that the magnitude of the expected magnetic fields (ignoring the geometric and other factors of order unity which we evaluate in this paper) is $\phi_0/a^2\times(e^2/amc^2)\sim 0.1$ T. Indeed, rather enormous fields might be expected.

The determination of the saddle point is now a straightforward task at zero temperature (we consider nonzero temperature later). The total-energy density E is given by

$$E=(4/J)|\chi|^2-(2/N)\sum_{\mathbf{k}}{}'\varepsilon(\mathbf{k})\ , \tag{11}$$

where N is the number of sites and the prime denotes a sum only over the filled states which is achieved by adjusting the chemical potential. Given a particular filling fraction, the energy can now be minimized numerically and the optimal value of $|\chi|$ and θ' found. We proceed by first fixing θ, the combined phase of $t\delta+\chi$. Then, for fixed θ, we optimize the energy with respect to θ' by inverting Eq. (6) to determine a constant value of $|\chi|$. Finally, the energy is optimized globally as a function of θ. The saddle-point value of $\theta(\delta)$ determines χ (and hence

the size of the circulating currents and real magnetic fields) as a function of doping. We plot $\theta(\delta)$ and $\theta'(\delta)$ in Fig. 2. The saddle-point value of θ decreases steadily away from π as the doping increases. At a doping of approximately $\delta=0.12$, the ground state undergoes a second-order transition to one with no flux: a free Fermi sea. The saddle-point energy is the sum of two parts: the hopping energy [the term in the Lagrangian (4) which is proportional to $t\delta$] and the magnetic exchange energy [the terms in (4) which involve χ_{xy}]. To emphasize the competition between hopping and exchange energies, we plot each in Fig. 3 in terms of the difference between the values calculated at the SFP saddle point and the values at the zero-flux saddle point (which is unstable for $\delta \lesssim 0.12$). In general, we see that nonzero flux favors the magnetic correlations and disfavors the hole kinetic energy.

III. REAL MAGNETIC FIELDS

The current on any link can be calculated by evaluating the rate of change of the expected number of electrons $\langle n_{\mathbf{x}} \rangle \equiv \langle c_{\mathbf{x}}^{\dagger\sigma} c_{\mathbf{x}\sigma} \rangle$ at site $\mathbf{x}$. (The bosons do not contribute to the electric current because they carry zero charge.) Actually, $\langle n_{\mathbf{x}} \rangle = 1-\delta$ is independent of time because currents $j_{\mathbf{xy}}$ flowing into the site through two of the links are balanced by currents flowing out through the other two links. Thus,

$$\sum_{\mathbf{y}}' j_{\mathbf{xy}} = \left\langle \frac{\partial}{\partial t} n_{\mathbf{x}} \right\rangle = i/\hbar \langle [H_{\mathrm{sp}}, n_{\mathbf{x}}] \rangle = i/\hbar \sum_{\mathbf{y}}' \langle (t\delta + \chi_{\mathbf{xy}}) c_{\mathbf{x}}^{\dagger\sigma} c_{\mathbf{y}\sigma} - \mathrm{H.c.} \rangle \ . \tag{12}$$

Here the prime denotes a sum over sites $\mathbf{y}$ that are neighbors of site $\mathbf{x}$. This expression may be simplified by using the equation of motion $\chi_{\mathbf{yx}} = (J/2) c_{\mathbf{x}}^{\dagger\sigma} c_{\mathbf{y}\sigma}$ to obtain the charge current along link $\langle \mathbf{xy} \rangle$:

$$j_{\mathbf{xy}} = \frac{4t\delta e}{\hbar J} \mathrm{Im}\chi_{\mathbf{xy}} \ . \tag{13}$$

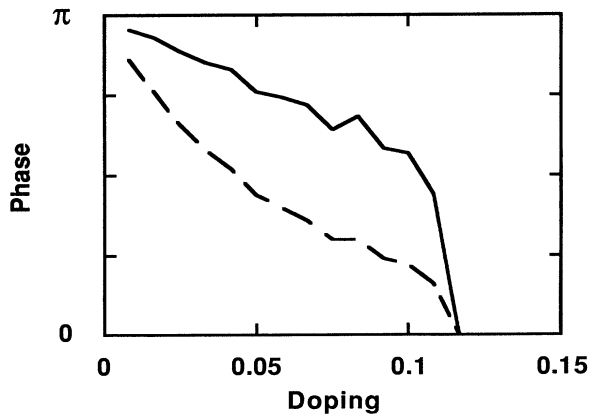

FIG. 2. Phases of $\bar{\chi}$ and χ vs doping. Solid line: θ'; dashed line: θ.

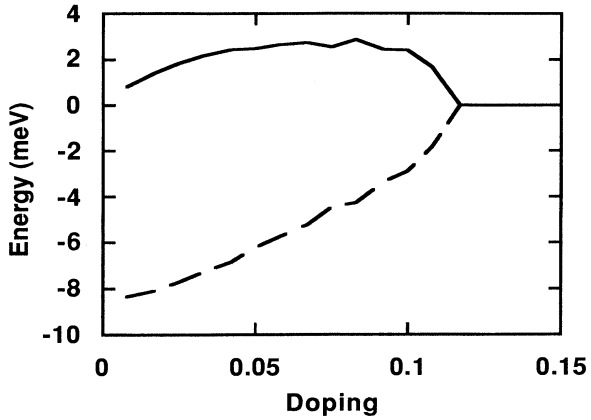

FIG. 3. Hopping and magnetic exchange energies per plaquette vs doping. Each is plotted as the difference between its value at the staggered-flux saddle point and at the zero-flux saddle point. Solid line: hopping energy; dashed line: magnetic energy.

Note that $\chi_{\mathbf{xy}} c_{\mathbf{x}}^{\dagger\sigma} c_{\mathbf{y}\sigma}$ has no imaginary part and so does not contribute to the charge current. The currents cease in either insulating limit ($\delta=0$ or $t=0$) reflecting the local gauge invariance that exists in pure antiferromagnet. The microscopic balance of the charge mentioned above is now apparent: at the saddle point, $\mathrm{Im}\chi_{\mathbf{xy}}$ is the same on every link up to a sign given by Fig. 1. Clearly these signs are such that no net currents flow into any site.

Using Eqs. (9) and (10) and substituting for the electron operators (see the Appendix for more details), the current can also be written

$$j_{\mathbf{xy}} = \frac{t\delta e}{\hbar} \sin\left[\frac{\theta}{4}\right] \frac{2}{N} \sum_{\mathbf{k}}' [\cos(k_y a) - \cos(k_x a)]^2 \times \langle \psi_-^{\dagger}(\mathbf{k}) \psi_-(\mathbf{k}) \rangle \Gamma(\mathbf{k},\theta)^{-1} \ . \tag{14}$$

[Γ was defined in Eq. (8).] This formula includes the sum over the spin; $\langle \psi_-^{\dagger}(\mathbf{k}) \psi_-(\mathbf{k}) \rangle$ picks out the ground-state occupation of single-particle states of either spin, and the prime means a sum over the reduced Brillouin zone. We see that states in the middle of the band contribute most to the orbital current. As we dope (increase δ) or raise the temperature, states near momenta $(\pm\pi/2a, \pm\pi/2a)$ are depleted first. The current, however, changes little (until the flux decreases) since these states contribute relatively less to the orbital current.

The current expressed as the magnetic field found at the center of a single arc of length and radius $a = 3.8$ Å is plotted in Fig. 4. Upon doping, the field rises and peaks at about 10 G. In order to convert the current into the magnetic field at a given point in the unit cell, we must sum over all nearby links of the CuO_2 lattice with the correct sense of the current direction. We sum these contributions numerically to determine a geometrical factor that multiplies the field strength plotted in Fig. 4. For points close to a link (Cu—O—Cu bond), the nonzero size of the Wannier functions is important. (If the currents were modeled by vanishingly thin wires, the

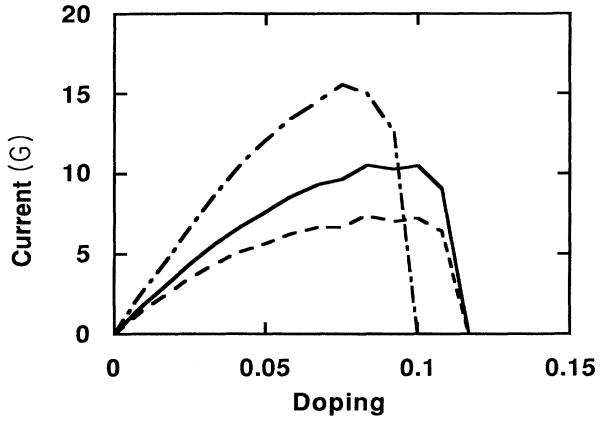

FIG. 4. Magnitude of current expressed in terms of a magnetic field (see text) vs doping. Solid line: mean-field approximation, zero temperature; dashed line: mean-field approximation but with electron occupancy given by the Fermi-Dirac distribution at a temperature of 150 K; dash-dotted line: Gutzwiller projection, zero temperature.

magnetic fields would diverge near the wires.) We model the distribution of currents in the CuO_2 planes with Wannier functions of size ξ by setting the current density equal to a constant for distances $r<\xi$ away from the Cu—O—Cu bond and zero outside this region. (For a single infinitely long bond, this ansatz clearly gives $H \propto I/r$ for $r>\xi$ and $H \propto Ir/\xi^2$ for $r<\xi$.) In Fig. 5 we plot the geometric factor for a doping of $\delta=0.1$ as a function of position for points near an oxygen atom (both in and out of the plane of the lattice). We have set ξ equal to the Cu—O separation ~ 2 Å to cut off the magnetic field at short distances. $\xi \sim 2$ Å is an upper bound because there is one Wannier orbital for each Cu atom and these atoms are separated by 4 Å. We consider the effect of different values for ξ later. To find the field at other dopings one simply rescales the fields plotted in Fig. 4.

In comparing the calculated fluxes to muon-spin-rotation experiments, there are several complications. In doped samples, the presence of superconductivity is one possible complication. However, since the energy scales of the staggered flux phase (t and J) are of order 1000 K, the SFP and its magnetic fluxes should be present at temperatures just above T_c. At nonzero temperatures,[22] the holes are not completely Bose condensed, complicating the calculation of the free energy. Based on our experience with the original large-n formulation of this problem (without the hole bosons), we expect, however, that the quantitative results of our zero-temperature calculation survive for temperatures $T \ll J/k_B \sim 1000$ K. We check the temperature dependence of the circulating current in a naive way by assuming the holes remain completely condensed in the lowest level (so that we may continue to set $b_x=\delta^{1/2}$), whereas the fermions occupy excited levels with a Fermi-Dirac distribution. We keep the flux fixed at the zero-temperature value and simply examine the effect of the Fermi-Dirac occupancy on the current, Eq. (14). The current at a temperature of $0.1J \sim 150$ K (again expressed as the magnetic field at the center of a single

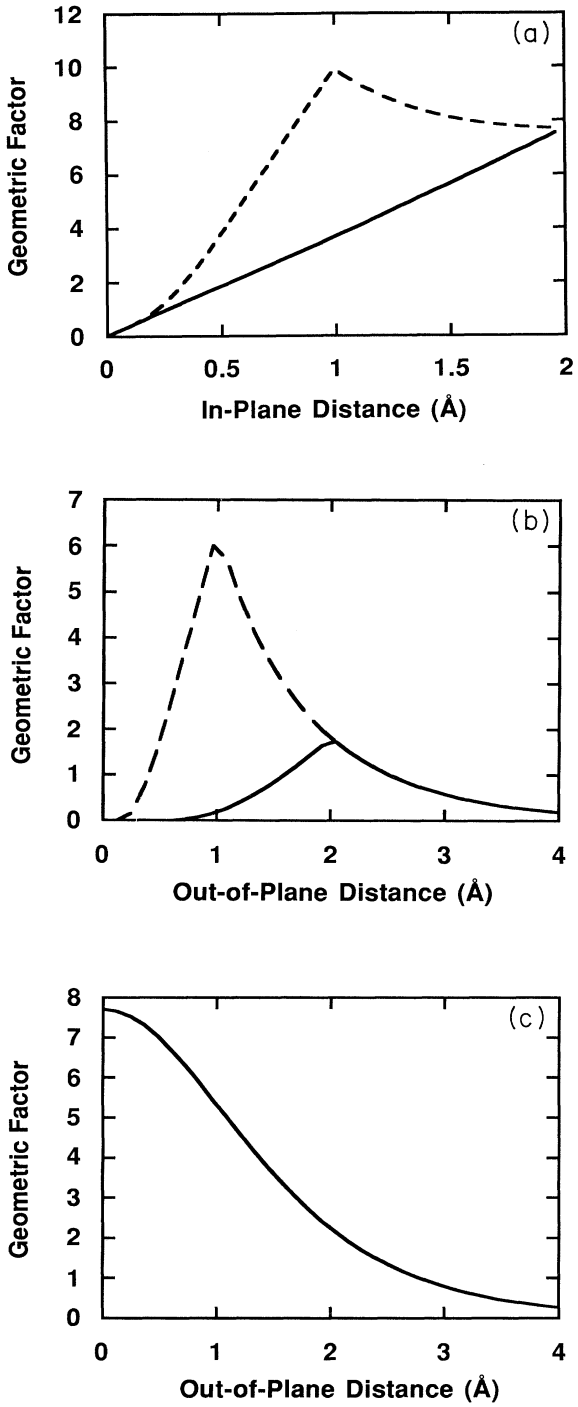

FIG. 5. Geometric factors for the magnetic field (see text). (a) $\hat{\mathbf{z}}$ component of the magnetic field at points in the CuO_2 plane near an oxygen atom as a function of perpendicular distance from the Cu—O bond. Other components of the magnetic-field vector are negligible. Solid line: $\xi=2.0$ Å; dashed line: $\xi=1.0$ Å. (b) Transverse component of the magnetic field at points vertically above a planar oxygen as a function of vertical distance. The $\hat{\mathbf{z}}$ component of the magnetic-field vector is negligible. Solid and dashed lines as in (a). (c) $\hat{\mathbf{z}}$ component field at the center of a plaquette as a function of vertical distance from the plane, independent of ξ.

arc) is plotted in Fig. 4. For small dopings there is very little change since the single-particle states near the Fermi level do not contribute much current [see the discussion following Eq. (14)]. However, at a doping of $\delta=0.1$, the current is suppressed by about 30%.

The muons may not see the magnetic fields if they prefer to lie far away from the CuO_2 planes or in some position of high symmetry. Kiefl *et al.*[23] and Brewer *et al.*[24] have recently studied muon-nuclear quadrupole level-crossing resonances in Y-Ba-Cu-O with ^{17}O substitution. Their results strongly suggest that the dominant muon site in Y-Ba-Cu-O is 1.0 Å away from a planar oxygen and on the outer side of the paired CuO_2 planes in the unit cell. (We study the expected magnetic fields near a planar oxygen for this reason.) Brewer *et al.* have also argued that the muon site is not likely to be close to the plane based on the internal fields observed by Birrer *et al.*[25] in Gd-Ba-Cu-O and the fact that an in-plane muon site is inconsistent with the observed isotropic copper nuclear dipole background.

The results plotted in Figs. 5(a) and 5(b) show that, if the muon lies in the CuO_2 plane, it could be in a field of 80 G at the optimum doping. If muons avoid the plane (the more likely case) and instead are bound to oxygens vertically above the plane, they would see fields of order 10 G. This latter value, owing to the steepness of the curve, is sensitive to the size of the Wannier functions. To understand the effect of our choice of Wannier function size ξ, we also plot the geometric factors for $\xi=1$ Å in Fig. 5. For this choice of ξ, fields of up to 60 G could be expected at the muon site. The field is very sensitive to ξ but it is probably fair to say that, without special tuning, transverse magnetics fields (parallel to the CuO_2 plane) of order tens of G should be seen by the muons. Note that, from Fig. 5(c), we can see that the contribution to the magnetic field from other layers is small—about 2–3 G if the layers are separated by 4 Å. This contribution decreases rapidly as the separation between layers increases.

Screening of the muon charge and muon-induced distortion of the Wannier functions is another complication. The positive muon charge probably suppresses the hole density near it. To see how the muon charge may change the local environment, we plot the geometric factor for the magnetic field, as in Fig. 5(b), but with the current in the nearest (vertically below) link turned off (see Fig. 6). This is presumably an extreme limit. Within our calculation, screening effects are uncertain because we do not have a good theory for hole dynamics. The resulting plots show that, at $\xi=2$ Å, turning off the link actually *increases* the expected field at the muon site by a factor of 3. This behavior has the following explanation: because the muon is well inside ξ (it is only 1 Å away from the bond), the contribution to the net field from the nearest link is, in fact, overwhelmed by contributions of opposite sign due to the next-nearest links. Thus, when the nearest link is turned off, the partial cancellation ceases and the magnetic field increases. If $\xi=1$ Å then the field is dominated by the nearest link and turning off the current in that link suppresses the field by a factor of 7. Nevertheless, in both cases we should still expect to see

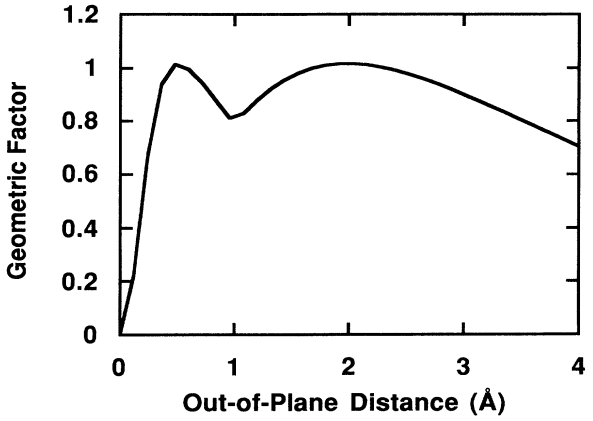

FIG. 6. Same geometric factor as in Fig. 5(b) but with the current in the nearest (vertically below) link turned off for both values of ξ.

field strengths of order 10 G at the optimum doping.

The most serious problem in comparing our calculation to muon experiments is the persistence of quasistatic spin moments at dopings of a few percent. According to neutron-scattering experiments on $YBa_2Cu_3O_x$ at various oxgyen concentrations,[26] long-range antiferromagnetic order disappears at a doping of about 2% which corresponds to an oxygen concentration of about 6.4. The disappearance of long-range order is deduced from the absence of Bragg scattering. Note, however, that quasistatic, but spatially disordered, spin moments may survive even if long-range order disappears. Between oxygen concentrations $x=6.4-6.5$, the doping rapidly rises by an additional 0.1–0.15 and T_c increases from 0 to 50 K. The effective doping is found by assuming that, at small doping, the spin-spin correlation length is given by $\delta=(a/\xi)^2$. Muon experiments on Y-Ba-Cu-O have examined the antiferromagnetism-superconductivity boundary and show that, as x increase from 6.4 to 6.5, the ordered magnetic field at the muon site drops from about 250 to 0 G. The rms deviation of the magnetic field peaks at about 50 G in the middle of this doping range.[27] The μSR samples and neutron-scattering samples show essentially the same dependence of T_c on oxygen concentration. That agreement provides some added confidence in the sample consistency.

If $x=6.4-6.5$ corresponds to hole concentrations in the range 0–0.1 (not unreasonable at all), then it may be impossible to see the staggered flux emerge from the sharply dropping background of the quasistatic spin moments. (We have no reason to believe that the muon site changes as one adds holes. We do not consider, however, secondary muon sites such as the one which lies in a field of 1300 G in the oxygen-depleted Néel phase.[28]). The peak in rms deviation in intriguing but could easily be caused by sample inhomogeneity. Actually, an intrinsic microscopic inhomogeneity probably arises from impurity potentials (especially due to random oxygen positions). At small doping these potentials may localize holes to within a few lattice sites. While this situation is not ac-

counted for explicitly in our calculation, it seems possible that hole localization might cause fields to appear at some muon positions and not at others.

In summary, there is no clear experimental evidence of a staggered flux from muon-spin-rotation data. However, because the size of the expected fields is small (of order 10 G), because quasistatic spin moments persist at nonzero doping, and because of the various theoretical uncertainties discussed in this section, we cannot rule out the SFP with the available observations. As a final remark, we note that static spin moments (for example, Néel order) and staggered fictitious flux are compatible, at least at half-filling.[10,29]

IV. NEUTRON SCATTERING

The pure two-dimensional nearest-neighbor spin-$\frac{1}{2}$ Heisenberg model is Néel ordered at zero temperature and exhibits a Bragg peak in the elastic spin-spin correlation function at momentum $(\pi/a,\pi/a)$. Neutron-scattering experiments on both the 2:1:4 and 1:2:3 materials show this peak,[30,31] and the dynamical behavior of the spin-wave excitations can be understood using the nonlinear σ model[32] or series expansions about the Ising limit.[33] The spin-spin correlations in the undoped flux phase were discussed in Ref. 4. The flux phase has no Néel order because the order parameter χ_{xy} is a singlet under SU(2) rotations. Indeed, the flux phase is a true spin liquid with no broken symmetries. (Since $\theta=\pi$ at $\delta=0$ and π flux is equivalent to $-\pi$ flux, translational symmetry is restored at half-filling.) But small peaks in the low-energy inelastic spin-spin correlations show up at momenta $(\pi/a,\pi/a)$, $(\pi/a,0)$, and $(0,\pi/a)$ [see Fig. 7(a)]. These peaks just reflect the fact that low-energy spin excitations occur only near the discrete Fermi points in the (undoped) flux phase. (For recent work on how Néel order may arise in the flux phase beyond the mean-field approximation, see Refs. 10 and 29.)

The nature of the spin-spin correlations at nonzero doping is more subtle because the mobile holes disorder the spins. To gain some understanding of how the flux phase incorporates the hole motion, we repeat the calculation of Ref. 4 but now at nonzero doping. We focus on low-energy spin excitations ($0<\omega\ll J$) since most of the neutron-scattering experiments are performed at low energy with respect to J. In addition to electron-hole pair excitations between the upper and lower bands, we also must include pairs that lie entirely within the lower band (for p-type doping) in our calculation of

$$S_\Delta(\mathbf{Q})\equiv(1/N)\sum_{\mathbf{x}} e^{i\mathbf{Q}\cdot\mathbf{x}}\langle \mathbf{S}_\mathbf{x}\cdot\mathbf{S}_0\rangle_\Delta \ .$$

Here $\mathbf{Q}$ is the scattering momentum and the subscript on the expectation values denotes an integration over ω (where ω is the decrease in the neutron energy due to the production of a spin excitation) with a Gaussian distribution $\exp-(\omega^2/2\Delta^2)$.

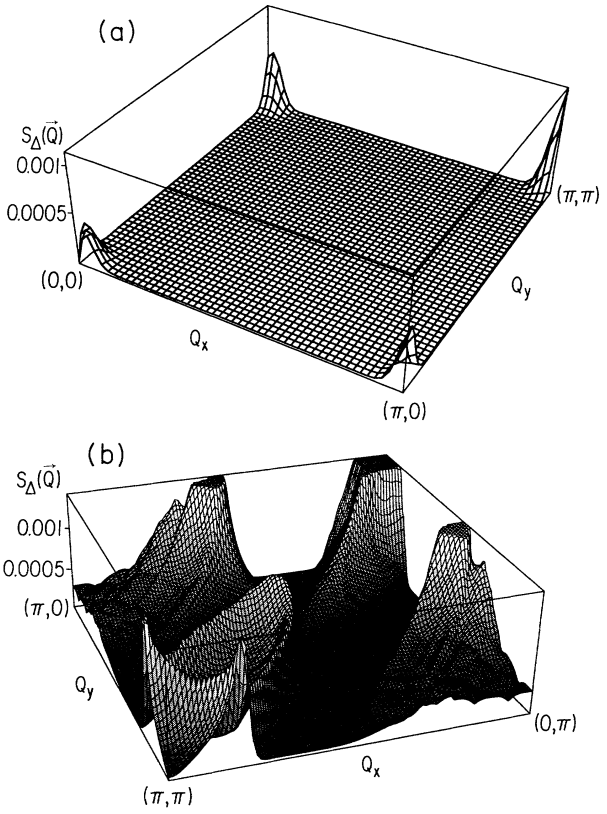

FIG. 7. Three-dimensional plots of the low-energy ($\Delta=6$ meV) inelastic spin-spin correlation function for (a) $\delta=0.0$ and (b) $\delta=0.075$.

We proceed by factorizing (using our mean-field approximation[4]) the required four-fermion expectation value into products of the terms like

$$\langle c_e^{\dagger\sigma}(\omega,\mathbf{k})c_{o\sigma}(\omega,\mathbf{k})\rangle$$

and

$$\langle c_e^{\dagger\sigma}(\omega,\mathbf{k})c_{e\sigma}(\omega,\mathbf{k})\rangle \ .$$

These expectation values can, in turn, be expressed using the occupation numbers in the upper and lower bands and the phase factor $g(\mathbf{k})$. The resulting formula for the zero-temperature spin-spin structure factor is given by an integral over the reduced Brillouin zone:

$$S_\Delta(\mathbf{Q})=\tfrac{3}{8}\int\frac{d^2p}{2\pi^2}\theta[\varepsilon(\mathbf{p})+\mu]([1-g^*(\mathbf{p}+\mathbf{Q})g(\mathbf{p})]\exp\{-[\varepsilon(\mathbf{p})+\varepsilon(\mathbf{p}+\mathbf{Q})]^2/2\Delta^2\}$$

$$+\theta[-\mu-\varepsilon(\mathbf{p}+\mathbf{Q})][1+g^*(\mathbf{p}+\mathbf{Q})g(\mathbf{p})]\exp\{-[\varepsilon(\mathbf{p})-\varepsilon(\mathbf{p}+\mathbf{Q})]^2/2\Delta^2\}) \ . \quad (15)$$

Here the step function $\theta(x)=1$ for $x>0$ and equals 0 for $x<0$. The structure factor for $\delta=0.075$ and $\Delta=6$ meV is plotted in Fig. 7(b). The splitting of the peak at momentum $\mathbf{Q}=(\pi/a,\pi/a)$ simply reflects the new length scale that has been introduced upon doping: the average separation between holes.

Quasielastic scattering is observed to persist at low doping in the 214 compound. In fact, neutron and muon experiments on a single $La_{1.94}Sr_{0.06}CuO_4$ sample demonstrated the existence of quasistatic but spatially disordered spin moments.[12] The quasielastic neutron-scattering intensity increased sharply as the sample temperature dropped from 40 to 20 K. The muons, on the other hand, saw the local spin moments freeze at around 6 K. This temperature difference was attributed to the slower response time of the muons to magnetic fluctuations mentioned in the Introduction. Evidently this glassy state, like the undoped Néel ordered phase, cannot be described by the highly inelastic processes in our mean-field approximation. Extensions of the nonlinear σ model that include holes seem better suited to describe this structure.[34] On the other hand, quasi-elastic scattering diminishes (possibly to zero) as the doping increases in both the 2:1:4 material[35] and the Y-Ba-Cu-O material.[26] So we might expect our theory to describe the spin excitations in this more highly doped (superconducting) region.

A splitting of the peak at the ordering wave vector $(\pi/a,\pi/a)$ has been seen in neutron-diffraction experiments on superconducting $La_{2-x}Sr_xCuO_{4-y}$ samples.[35] (No such splitting was seen in superconducting Y-Ba-Cu-O compounds.[26]) However, the observed neutron scattering may be too strong to be explained by highly inelastic processes predicted by our mean-field theory. The experiments typically scan along the line that connects (0,0) with $(\pi/a,\pi/a)$. But the additional structure along the $Q_x=0$ and $Q_y=0$ axes shown in Fig. 7(b) has not been observed.

Neutrons interact not only with the magnetic moment of electron spins, but also with the magnetic fields produced by the orbital currents. Since these currents preserve the $\sqrt{2}$ unit cell, Bragg scattering at momentum $(\pi/a,\pi/a)$ will occur. To determine whether it is possible to separate this orbital contribution from quasistatic spin-moment scattering, we ignore interference between these two processes and consider the (spin-independent) coupling of electrons on a given link to the gauge field of the neutron magnetic moment:

$$t\delta c_{\mathbf{x}}^{\dagger\sigma}c_{\mathbf{y}\sigma}\exp\left[i\frac{e}{\hbar c}\int_{\mathbf{x}}^{\mathbf{y}}\mathbf{A}\cdot d\mathbf{l}\right] . \tag{16}$$

Here $\mathbf{x}$ and $\mathbf{y}$ are nearest-neighbor sites. The neutron magnetic moment

$$\boldsymbol{\mu}=-1.91\frac{e\hbar}{m_n c}\mathbf{S} \tag{17}$$

produces a gauge field

$$\mathbf{A}=\boldsymbol{\mu}\times(\mathbf{r}_{\text{electron}}-\mathbf{r}_{\text{neutron}})/|\mathbf{r}_e-\mathbf{r}_n|^3 . \tag{18}$$

The first approximation we make is to cut off $|\mathbf{r}_e-\mathbf{r}_n|$ at about $d=1$ Å (roughly the size of the Wannier functions). Because

$$\int \mathbf{A}\cdot d\mathbf{l}\sim(e^2/d)\cdot(m_n c^2)^{-1}\ll 1 ,$$

the coupling simplifies to

$$i\frac{t\delta e}{\hbar c}c_{\mathbf{x}}^{\dagger\sigma}c_{\mathbf{y}\sigma}\int_{\mathbf{x}}^{\mathbf{y}}\mathbf{A}\cdot d\mathbf{l} . \tag{19}$$

Substituting for $\mathbf{A}$ we find

$$\int_{\mathbf{x}}^{\mathbf{y}}\mathbf{A}\cdot d\mathbf{l}=\int_0^a dw\frac{\mathbf{R}_{\mathbf{x}}+w\hat{\mathbf{e}}-\mathbf{r}_n}{|\mathbf{R}_{\mathbf{x}}+w\hat{\mathbf{e}}-\mathbf{r}_n|^3}\cdot(\hat{\mathbf{e}}\times\boldsymbol{\mu}) , \tag{20}$$

where $\mathbf{R}_{\mathbf{x}}$ is the position of the ith site and the unit vector $\hat{\mathbf{e}}$ runs from $\mathbf{x}$ to $\mathbf{y}$. Sandwiching this expression between initial and final neutron states with $\mathbf{k}_i-\mathbf{k}_f\equiv\mathbf{q}$ and integrating over the neutron coordinates, we obtain

$$(1/V)\int d^3\mathbf{r}_n e^{i\mathbf{q}\cdot\mathbf{r}_n}\int_{\mathbf{x}}^{\mathbf{y}}\mathbf{A}\cdot d\mathbf{l}$$
$$=(4\pi/Vq^2)e^{i\mathbf{q}\cdot\mathbf{R}_{\mathbf{x}}}(1-e^{i\mathbf{q}\cdot a\hat{\mathbf{e}}})\frac{\hat{\mathbf{e}}\cdot(\boldsymbol{\mu}\times\mathbf{q})}{\mathbf{q}\cdot\hat{\mathbf{e}}} , \tag{21}$$

where $V=L_xL_yL_z$ is the volume of the system.

For now we pull out a factor $\exp(iq_zR_{\mathbf{x}}^z)L_z^{-1}$ from this expression. We shall reinsert it when we consider Bragg scattering from more than one CuO_2 layer. The next step is to sum over all the links of the lattice and substitute the electron eigenfunctions $\psi_\pm$ for both spins. Writing only the relevant parts (we drop the spin index for the moment):

$$\sum_{\mathbf{x}}\sum_{\hat{\mathbf{e}}=\hat{\mathbf{x}},\hat{\mathbf{y}}}e^{i\mathbf{q}\cdot\mathbf{R}_{\mathbf{x}}}(1-e^{i\mathbf{q}\cdot a\hat{\mathbf{e}}})(c_{\mathbf{x}+a\hat{\mathbf{e}}}^{\dagger}c_{\mathbf{x}}-c_{\mathbf{x}}^{\dagger}c_{\mathbf{x}+a\hat{\mathbf{e}}})$$
$$=\sum_{\mathbf{k}}\sum_{\hat{\mathbf{e}}=\hat{\mathbf{x}},\hat{\mathbf{y}}}c_{\mathbf{k}+\mathbf{q}}^{\dagger}c_{\mathbf{k}}2[\cos(\mathbf{k}\cdot a\hat{\mathbf{e}})-\cos(\mathbf{k}\cdot a\hat{\mathbf{e}}+\mathbf{q}\cdot a\hat{\mathbf{e}})]$$
$$=\sum_{\mathbf{k}}'\sum_{\hat{\mathbf{e}}=\hat{\mathbf{x}},\hat{\mathbf{y}}}2[c_e^{\dagger}(\mathbf{k}+\mathbf{q})c_o(\mathbf{k})+c_o^{\dagger}(\mathbf{k}+\mathbf{q})c_e(\mathbf{k})][\cos(\mathbf{k}\cdot a\hat{\mathbf{e}})-\cos(\mathbf{k}\cdot a\hat{\mathbf{e}}+\mathbf{q}\cdot a\hat{\mathbf{e}})]$$
$$=\sum_{\mathbf{k}}'\sum_{\hat{\mathbf{e}}=\hat{\mathbf{x}},\hat{\mathbf{y}}}[\cos(\mathbf{k}\cdot a\hat{\mathbf{e}})-\cos(\mathbf{k}\cdot a\hat{\mathbf{e}}+\mathbf{q}\cdot a\hat{\mathbf{e}})][g(\mathbf{k})+g^*(\mathbf{k}+\mathbf{q})][\psi_-^{\dagger}(\mathbf{k}+\mathbf{q})\psi_-(\mathbf{k})+\psi_+^{\dagger}(\mathbf{k}+\mathbf{q})\psi_-(\mathbf{k})+\cdots] . \tag{22}$$

The primes indicate the sum is over the reduced Brillouin zone. For Bragg scattering (q_x,q_y) is a multiple of $(\pi/a,\pi/a)$,

$$g(\mathbf{k})+g^*(\mathbf{k}+\mathbf{q})=2i\sin(\theta/4)(\cos k_x a-\cos k_y a)\Gamma(\mathbf{k},\theta)^{-1} \tag{23}$$

and $[\cos\mathbf{k}\cdot a\hat{\mathbf{e}}-\cos(\mathbf{k}\cdot a\hat{\mathbf{e}}+\mathbf{q}\cdot a\hat{\mathbf{e}})]=2\cos(\mathbf{k}\cdot a\hat{\mathbf{e}})$. The Bragg-scattering matrix element is

$$\frac{16\pi et\delta}{\hbar cN}\sum_{\mathbf{k}}{}'\langle\psi_-^\dagger(\mathbf{k}+\mathbf{q})\psi_-(\mathbf{k})\rangle\sin(\theta/4)\Gamma^{-1}(\mathbf{k},\theta)(\cos k_y a-\cos k_x a)\sum_{\hat{\mathbf{e}}=\hat{\mathbf{x}},\hat{\mathbf{y}}}\frac{\hat{\mathbf{e}}\cdot(\boldsymbol{\mu}\times\mathbf{q})}{(a\mathbf{q})^2\mathbf{q}\cdot\hat{\mathbf{e}}}\ . \tag{24}$$

Converting this to a cross section, averaging over the neutron spin, substituting for $t\equiv\hbar^2/2m^*a^2$, multiplying by 2 to account for electron spin, and finally assuming that there is no momentum transfer in the $\hat{\mathbf{z}}$ direction, we obtain

$$\frac{d\sigma}{d\Omega}=\left[\frac{1.91e^2}{mc^2}\right]^2\left[\frac{m}{m^*}\right]^2\left|\delta\frac{2}{N}\sum_{\mathbf{k}<\mathbf{k}_F}{}'\sin(\theta/4)\Gamma^{-1}(\mathbf{k},\theta)(\cos k_x a-\cos k_y a)^2\right|^2\frac{2}{(a\mathbf{q})^2}\ . \tag{25}$$

The quantity $|\delta\cdots|$ may be estimated by noting that it is the current plotted in Fig. 4 multiplied by $\hbar ac/te=3.5\times10^{-3}\ \mathrm{G}^{-1}$. Thus, the quantity $|\delta\cdots|$ has a peak value of around 0.037 at optimum doping. For the case of scattering at $(\pi/a,\pi/a,0)$, the rest of the dimensionless terms contribute a factor ~0.42. So altogether we have a numerical factor 5.7×10^{-4} multiplying $(1.91e^2/mc^2)^2$.

Let us compare these numbers to the cross section for Bragg scattering from the spins. In this case,

$$\frac{d\sigma}{d\Omega}=\left[\frac{1.91e^2}{mc^2}\right]^2\langle S_z\rangle^2|f(\mathbf{q})|^2\ . \tag{26}$$

The magnetic structure factor for copper spins in K_2CuF_4 was measured by Akimitsu and Ito.[36] Interpolating their data for our scattering wave vector, the structure factor is $f(\mathbf{q})\sim0.8$. For an ordered moment of 50%, $\langle S_z\rangle\sim0.25$ and the total numerical factor is 4.0×10^{-2}. This number is about 70 times greater than scattering from orbital moments. This large factor comes from the fact that orbital moments are proportional to the doping $\delta\sim0.1$ so the scattering intensity is proportional to the square of the doping. The expected Bragg peak intensity is below the resolution presently achieved by neutron-scattering experiments.

Bearing in mind the preceding result let us, nevertheless, consider nonzero-momentum transfer in the $\hat{\mathbf{z}}$ direction. To be definite, let us suppose that the flux from adjacent layers is opposite in sign (in analogy with the spin moments in the Néel ordered state), causing a cancellation if $q_z=0$. We shall show that such behavior should manifest itself in the behavior of the scattering amplitude as a function of q_z. Let us consider the case of Y-Ba-Cu-O at scattering wave vectors $\mathbf{q}=(\pi/a,\pi/a,2\pi n/c)$. We take $c=11.8$ Å to be the unit-cell dimension perpendicular to the planes. Because adjacent planes (which are separated by $z=3.4$ Å) have opposite flux, $\sin(\theta/4)$ changes sign between the two planes. Since we are considering Bragg scattering, the neutron spin is conserved. Spin-flip processes have a different q_z dependence and, in fact, this different q_z dependence was originally used to deduce that the Néel ordering direction is parallel to the CuO_2 planes.[31]

Note that the only q_z dependences come from the $q/(a\mathbf{q})^2$ term in Eq. (25) and $\exp(iq_zR_{\mathbf{x}}^z)L_z^{-1}$ which we factored out earlier. The scattering cross section is thus proportional to

$$|1-e^{i2\pi nz/c}|^2/[2\pi^2+(2\pi na/c)^2]^2\ . \tag{27}$$

For $n=0$, 1, 2, and 3, the relative amplitudes are 0, 0.42, 0.26, and 0.06. This n dependence would be a signature of an orbital moment pointing in the $\hat{\mathbf{z}}$ direction. Again, the expected magnitude for this signal is probably too small to be observed.

V. CONCLUSIONS

Unlike the anyon[19] and commensurate-flux[21] theories of the high-temperature superconductors, our mean-field theory exhibits real magnetic fields only at low doping ($0<\delta<0.12$). Without special tuning we expect fields of order 10 G to appear. There are a number of uncertainties including (a) whether the actual doping in a given experimental sample is uniform and close to the optimum doping 0.1, (b) hole localization at low doping due to microscopic (mostly oxygen) inhomogeneity, (c) the actual size of the Wannier function carrying the current and how the muon may distort it, (d) screening of the muon charge, (e) nonzero temperature, and (f) the validity of the mean-field approximation itself. Note, however, that the Gutzwiller projection approach yields similar values for the magnetic field (see the Appendix).

Local spin moments are observed to persist at nonzero doping and may mask the orbital magnetic moments (if they exist) at the muon site. At present we can only conclude that the muon experiments do not rule out the staggered flux phase. However, it may be possible to use the different response times of muons and neutrons to fluctuating magnetic fields to set more stringent bounds on the static orbital contribution. Finally, the orbital moment is too small to be observed directly by neutron Bragg scattering.

On the other hand, our mean-field theory clearly does not reproduce the quasistatic spin moments observed at low doping. Néel order may be incorporated into the undoped flux phase by giving the fermions a mass gap;[10,29] whether this hybrid can explain features at nonzero doping like the disordered static spin moments or the incommensurate spin structure remains to be seen. The fact that the SFP inelastic structure shows some qualitative similarities with neutron experiments on the superconducting 2:1:4 samples suggests that such a fusion might be possible. We also note that the staggered flux phase

shares some features with the "double-spiral" phase of Kane *et al.*:[37] both phases exhibit staggered chiral spin order which changes sign upon translation by one site or time reversal.

For dopings greater than about 12%, the currents in our mean-field theory cease to flow and the magnetic fields vanish. Muon-spin-rotation experiments in this (superconducting) region set a stringent upper bound (less than half a G) on the allowed local magnetic fields and seem to rule out anyon and commensurate-flux theories.[23] But the measurements appear to be consistent with the zero-flux Fermi-liquid phase. Furthermore, the quasistatic spin moment diminishes with increasing hole concentration,[26,35] so our spin-liquid phases are better suited to this region. Finally, recent work by Grilli and Kotliar[14] suggests that the Fermi-liquid phase could support a superconducting condensate.

Note added in proof. If we included next-nearest-neighbor hopping $t_{\rm NNN}=0.06$ eV in the mean-field theory, then the critical value of the doping at which the flux vanishes is reduced slightly to $\delta\approx 0.10$.

ACKNOWLEDGMENTS

We thank J. Brewer, W. J. L. Buyers, R. Kiefl, G. Kotliar, G. Luke, D. Rokhsar, and E. Siggia for helpful discussions and W. Unruh for technical assistance. This work was supported by the Natural Sciences and Engineering Research Council of Canada (I.A., T.C.H.), the Killam Foundation (T.C.H.), and IBM (J.B.M.).

APPENDIX

The calculations presented in this paper are justified in a large-n limit. In this section we perform instead a variational calculation using a Gutwziller-projection scheme. With this technique we find similar values for the real magnetic fields as a function of doping. We also obtain fairly accurate values for the magnetic and hole kinetic energies near half-filling. The philosophy behind this approach is the following: since we wish to compute physical quantities, we ought to minimize the variational energy of a physically sensible ground state with respect to a physically sensible Hamiltonian. Here we choose our variational wave function to be Gutzwiller-projected noninteracting electrons moving in the staggered flux. (Before projection, the electrons occupy the lowest single-particle states.) This wave function is a physically sensible variational ground state because it strictly obeys the single occupancy constraint—there is either a hole or an electron at each site. (The saddle-point approach only satisfies the constraint on average.) We calculate the kinetic and magnetic energies variationally with respect to the t-J Hamiltonian and then adjust the staggered flux in order to minimize the total energy.

The Gutzwiller-projection operator

$$P_G=\prod_{\text{sites } \mathbf{x}} P_G^{\mathbf{x}}=\prod_{\text{sites } \mathbf{x}}(1-n_{\mathbf{x}\uparrow}n_{\mathbf{x}\downarrow}) \tag{A1}$$

is approximated by dividing the lattice into two sets of sites. In this calculation they will consist of two adjacent sites (set B) and all other sites (set A). Let us also decompose the projection on set B into

$$\prod_{\mathbf{x}\in B}(1-n_{\mathbf{x}\uparrow}n_{\mathbf{x}\downarrow})=\sum_{n=1}^{9} Q_n \ , \tag{A2}$$

where Q_n are projection operators onto the 3^2 possible real-space configurations [(1) up spin, (2) down spin, and (3) empty site] on the two sites of set B. The matrix element of some operator $\mathcal{O}$, which acts on the sites of B, is

$$\mathcal{M}=\frac{\sum_{n,n'}\left\langle \prod_{\mathbf{x}\in A} P_G^{\mathbf{x}} Q_n \mathcal{O} Q_{n'}\right\rangle}{\sum_{n}\left\langle \prod_{\mathbf{x}\in A} P_G^{\mathbf{x}} Q_n\right\rangle} \ . \tag{A3}$$

Evaluation of the matrix elements of operators acting on set B is easy because we are evaluating expectation values of two-body correlations for free electrons. The difficult factor to evaluate is $\prod_{\mathbf{x}\in A}P_G^{\mathbf{x}}$ which is the conditional probability that the expectation value of $\prod_{\mathbf{x}\in A}P_G^{\mathbf{x}}$ is nonzero given that a certain configuration of up spins, down spins, and holes exists on B. We evaluate it very crudely.

Let N be the total number of sites and $N_{A,B}^{\sigma}$ be the number of electrons of spin σ on set A,B. We assume zero magnetization so that

$$N_A^{\sigma}+N_B^{\sigma}=N^{\sigma}+N(1-\delta)/2 \ .$$

The number of real space configurations of spin σ electrons on A is

$$\frac{N_A!}{N_A^{\sigma}!(N_A-N_A^{\sigma})!} \ . \tag{A4}$$

We assume that they all have equal weight—that is, we neglect the quantum degeneracy pressure of set A. For every spin-σ configuration only

$$\frac{(N_A-N_A^{-\sigma})!}{N_A^{\sigma}!(N_A-N_A^{\sigma}-N_A^{-\sigma})!} \tag{A5}$$

configurations manage to avoid all the spin-σ electrons. Therefore, the probability of a nonzero result after projection is simply (A5) divided by (A4), or,

$$\frac{(N_A-N_A^{\uparrow})!(N_A-N_A^{\downarrow})!}{N_A!(N_A-N_A^{\uparrow}-N_A^{\downarrow})!} \ . \tag{A6}$$

The effect of $\prod_{\mathbf{x}\in A}P_G^{\mathbf{x}}$ is simply to introduce a fugacity for holes. Suppose we decrease the number of up-spin electrons on set B by one thereby increasing the number of up-spin electrons on set A by one. Then, the above probability changes by

$$\frac{(N_A-N_A^{\uparrow}-N_A^{\downarrow})}{(N_A-N_A^{\uparrow})}=\frac{2\delta}{1+\delta}+O(1/N) \ . \tag{A7}$$

We may now write down our analytic approximations for projected matrix elements. We first calculate (unnormalized) probabilities for various spatial configurations of electrons on the two adjacent sites of set B. We shall use the notation $P(\uparrow,0)$ (introduced in Refs. 9 and 10) to denote the probability that on set B we have, say, an up spin on site $\mathbf{x}$ and a hole on site $\mathbf{x}+\hat{\mathbf{e}}$. For example,

$$P(\uparrow\uparrow)\equiv\langle|P_G n_{\mathbf{x},\uparrow}(1-n_{\mathbf{x},\downarrow})n_{\mathbf{x}+\hat{\mathbf{e}},\uparrow}(1-n_{\mathbf{x}+\hat{\mathbf{e}},\downarrow})P_G|\rangle$$
$$\approx\langle n_{\mathbf{x},\uparrow}n_{\mathbf{x}+\hat{\mathbf{e}},\uparrow}\rangle\langle(1-n_{\mathbf{x},\downarrow})(1-n_{\mathbf{x}+\hat{\mathbf{e}},\downarrow})\rangle\ , \tag{A8}$$
$$P(\uparrow 0)\equiv\langle|P_G n_{\mathbf{x},\uparrow}(1-n_{\mathbf{x},\downarrow})(1-n_{\mathbf{x}+\hat{\mathbf{e}},\uparrow})(1-n_{\mathbf{x}+\hat{\mathbf{e}},\downarrow})P_G|\rangle$$
$$\approx\langle n_{\mathbf{x},\uparrow}n_{\mathbf{x}+\hat{\mathbf{e}},\uparrow}\rangle\langle(1-n_{\mathbf{x},\downarrow})(1-n_{\mathbf{x}+\hat{\mathbf{e}}f,\downarrow})\rangle\times\frac{2\delta}{1+\delta}\ , \tag{A9}$$

where $\langle\ \rangle$ denotes an expectation value for the free electrons before projection (in this situation, spin independent). In order to calculate some particular matrix element, one would normalize by the sum of the nine such probabilities $P(\cdots)$.

Let us calculate some quantities for electrons in a staggered-flux ground state. One such expectation value that appears in the formulas for the kinetic energy, current, and magnetic exchange energy is

$$\frac{2}{N}\sum_{\mathbf{x}\ \text{even}}\langle c^\dagger_{\mathbf{x}}c_{\mathbf{x}+a\hat{\mathbf{e}}}\rangle=\frac{2}{N}{\sum_{\mathbf{k}}}'\langle c^\dagger_e(\mathbf{k})c_o(\mathbf{k})e^{i\mathbf{k}\cdot a\hat{\mathbf{e}}}\rangle$$
$$=-\frac{2}{N}{\sum_{\mathbf{k}}}'\frac{e^{i\mathbf{k}\cdot a\hat{\mathbf{e}}}}{2g(\mathbf{k})}\langle\psi^\dagger_-(\mathbf{k})\psi_-(\mathbf{k})\rangle\ . \tag{A10}$$

We have dropped the spin index; instead of summing over it we are now considering each spin separately. Again the prime means the sum is restricted to the reduced Brillouin zone.

Another useful quantity is the nearest-neighbor density-density correlation $\langle c^\dagger_{\mathbf{x}+a\hat{\mathbf{e}}}c_{\mathbf{x}+a\hat{\mathbf{e}}}c^\dagger_{\mathbf{x}}c_{\mathbf{x}}\rangle$ (for either spin species). Its value is n_σ^2-x, where the exchange hole x is given by

$$x=\left|\frac{1}{N}{\sum_{\mathbf{k}}}'\langle\psi^\dagger_-\psi_-\rangle e^{i\mathbf{k}\cdot a\hat{\mathbf{e}}}g(\mathbf{k},\theta)\right|^2\ . \tag{A11}$$

Using these quantities and setting $n_\sigma=n=(1-\delta)/2$, we may calculate the unnormalized probabilities

$$P(\uparrow\uparrow)\sim(n^2-x)[(1-n)^2-x]\ ,$$
$$P(\uparrow\downarrow)\sim(n-n^2+x)^2\ ,$$

and so on. The normalization factor $\sum P(\ )$ is, to lowest order in δ and x,

$$\sum P(\ )=\tfrac{1}{4}+\tfrac{1}{2}\delta+\tfrac{3}{4}\delta^2+4x^2\ .$$

Using the projection prescription to calculate the current or kinetic energy simply requires that we multiply the free-electron expression for spin σ by

$$\left[\frac{2\delta}{1+\delta}\right]\frac{\langle(1-n_{\mathbf{x},-\sigma})(1-n_{\mathbf{x}+a\hat{\mathbf{e}},-\sigma})\rangle}{\sum P}\ , \tag{A12}$$

where

$$\langle(1-n_{\mathbf{x},-\sigma})(1-n_{\mathbf{x}+a\hat{\mathbf{e}},-\sigma})\rangle=\left[\frac{1+\delta}{2}\right]^2-x\ . \tag{A13}$$

The factor (A12) can be viewed as a renormalization of t:

$$t\to\tilde{t}=t\cdot 2\delta(1-4x+12\delta x-16x^2)\ .$$

The charge current in the $\hat{\mathbf{e}}$ direction (from even to odd sublattice) is then:

$$j_{\hat{\mathbf{e}}}=\frac{i\tilde{t}e}{\hbar}\frac{2}{N}{\sum_{\mathbf{k}}}'\langle c^\dagger_{\mathbf{x}+a\hat{\mathbf{e}}}c_{\mathbf{x}}-c^\dagger_{\mathbf{x}}c_{\mathbf{x}+a\hat{\mathbf{e}}}\rangle$$
$$=\frac{i\tilde{t}e}{\hbar}\frac{1}{N}{\sum_{\mathbf{k}}}'e^{i\mathbf{k}\cdot a\hat{\mathbf{e}}}[g^*(\mathbf{k})-g(\mathbf{k})]$$
$$\times\langle\psi^\dagger_-(\mathbf{k})\psi_-(\mathbf{k})\rangle\ . \tag{A14}$$

Multiplying by an additional factor of 2 to take into account the two spin species and substituting for $g(\mathbf{k})$, the expression for current in a link becomes

$$-2\frac{\tilde{t}e}{\hbar}\sin\left[\frac{\theta}{4}\right]\frac{2}{N}{\sum_{\mathbf{k}}}'e^{i\mathbf{k}\cdot a\hat{\mathbf{e}}}[\cos(k_y a)-\cos(k_x a)]$$
$$\times\langle\psi^\dagger_-(\mathbf{k})\psi_-(\mathbf{k})\rangle\Gamma(\mathbf{k},\theta)^{-1}\ . \tag{A15}$$

In the ground state $\langle\psi^\dagger_-(\mathbf{k})\psi_-(\mathbf{k})\rangle$ is invariant under $\mathbf{k}\to-\mathbf{k}$ and $k_x\leftrightarrow k_y$ so that the expression for current simplifies to

$$\frac{\tilde{t}e}{\hbar}\sin\left[\frac{\theta}{4}\right]\frac{2}{N}{\sum_{k<k_F}}'[\cos(k_y a)-\cos(k_x a)]^2\Gamma(\mathbf{k},\theta)^{-1}\ . \tag{A16}$$

The kinetic energy per plaquette, defined by

$$E_{\text{kin}}\equiv t\langle P_G(c^\dagger_{\mathbf{x}}c_{\mathbf{y}}+\text{H.c.})P_G\rangle\ ,$$

summed over both spins is

$$E_{\text{kin}}=-2\tilde{t}\cos\left[\frac{\theta}{4}\right]\frac{2}{N}{\sum_{\mathbf{k}}}'[\cos(k_x a)+\cos(k_y a)]^2$$
$$\times\langle\psi^\dagger_-(\mathbf{k})\psi_-(\mathbf{k})\rangle\Gamma(\mathbf{k},\theta)^{-1}\ . \tag{A17}$$

The magnetic exchange energy as a function of flux and doping is made easier to calculate because the ground state is a singlet,

$$E_{\text{mag}}\equiv J\langle\mathbf{S}_{\mathbf{x}}\cdot\mathbf{S}_{\mathbf{x}+a\hat{\mathbf{e}}}\rangle$$
$$=3J\langle S^z_{\mathbf{x}}S^z_{\mathbf{x}+a\hat{\mathbf{e}}}\rangle$$
$$=\frac{3J}{4}\times\left[\frac{P(\uparrow\uparrow+P(\downarrow\downarrow)-P(\uparrow\downarrow)-P(\downarrow\uparrow)}{\sum P(\ )}\right]\ . \tag{A18}$$

The variational calculation proceeds in the following way: for a fixed value of hole concentration δ, the phase

$\theta(\delta)$ which minimizes $E_{\rm kin}+E_{\rm mag}$ is found. For that value of $\theta(\delta)$ the absolute current in a link is calculated. The resulting current is plotted in Fig. 4. Like the large-n limit, the ground state becomes one with no flux (that is, a projected free Fermi sea) at a doping of about 0.10. The main difference is that the current has a maximum of about 15 G (50% larger than at large n) at a doping of about 7.5%. These results give some insight into the quantitative limitations of the large-n mean-field approximation.

[1]P. W. Anderson, Science **235**, 1196 (1987).
[2]G. Kotliar, Phys. Rev. B **37**, 3664 (1988).
[3]I. Affleck and J. B. Marston, Phys. Rev. B **37**, 3774 (1988).
[4]J. B. Marston and I. Affleck, Phys. Rev. B **39**, 11 538 (1989).
[5]F. C. Zhang *et al.*, Supercond. Sci. Tech. **1**, 36 (1988).
[6]F. C. Zhang, Phys. Rev. Lett. **64**, 974 (1990).
[7]C. Gros, Ann. Phys. (N.Y.) **189**, 53 (1989); Phys. Rev. B **38**, 931 (1988).
[8]T.-K. Lee and S.-P. Feng, Phys. Rev. B **38**, 11 809 (1988).
[9]T. C. Hsu, Ph.D. thesis, Princeton University, 1989.
[10]T. C. Hsu, Phys. Rev. B **41**, 11 379 (1990).
[11]Z. Wang, G. Kotliar, and X. Wang, Phys. Rev. B **42**, 8690 (1990).
[12]B. J. Sternlieb *et al.*, Phys. Rev. B **41**, 8866 (1990).
[13]T. Dombre and G. Kotliar, Europhys. Lett. **10**, 667 (1989).
[14]M. Grilli and G. Kotliar, Phys. Rev. Lett. **64**, 1170 (1990).
[15]M. S. Hybertsen *et al.*, Phys. Rev. B **41**, 11 068 (1990).
[16]R. R. P. Singh, *et al.*, Phys. Rev. Lett. **62**, 2736 (1989).
[17]T. Dombre and G. Kotliar, Phys. Rev. B **39**, 855 (1989).
[18]S. Sachdev, Phys. Rev. B **41**, 1445 (1990).
[19]R. B. Laughlin, Phys. Rev. Lett. **60**, 1057 (1988).
[20]F. Nori and G. Zimanyi (unpublished).
[21]P. Lederer, D. Poilblanc, and T. M. Rice, Phys. Rev. Lett. **63**, 1519 (1989).
[22]See Ref. 4 and A. B. Harris *et al.*, Phys. Rev. B **40**, 2631 (1989) for a treatment of nonzero temperature in a model with no slave bosons.
[23]R. F. Kiefl *et al.*, Phys. Rev. Lett. **64**, 2082 (1990).
[24]J. H. Brewer *et al.* (unpublished).
[25]P. Birrer *et al.*, Phys. Rev. B **39**, 11 449 (1989).
[26]J. Rossat-Mignod *et al.* (unpublished).
[27]R. F. Kiefl *et al.*, Phys. Rev. Lett. **63**, 2136 (1989).
[28]J. H. Brewer *et al.*, Physica C **162-164**, 157 (1989).
[29]J. B. Marston, Phys. Rev. Lett. **64**, 1166 (1990); J. B. Marston, Phys. Rev. B **42**, 10 804 (1990).
[30]G. Shirane *et al.*, Phys. Rev. Lett. **59**, 1613 (1987); Y. Endoh *et al.*, Phys. Rev. B **37**, 7443 (1988).
[31]J. M. Tranquada *et al.*, Phys. Rev. Lett. **60**, 156 (1988).
[32]S. Chakravarty, B. I. Halperin, and D. R. Nelson, Phys. Rev. Lett. **60**, 1057 (1988); S. Chakravarty (unpublished).
[33]R. R. P. Singh, Phys. Rev. B **39**, 9760 (1989); R. R. P. Singh and D. A. Huse, *ibid.* **40**, 7247 (1989).
[34]B. I. Shraiman and E. D. Siggia, Phys. Rev. Lett. **61**, 467 (1988).
[35]G. Shirane *et al.*, Phys. Rev. Lett. **63**, 330 (1989); T. R. Thurston *et al.*, Phys. Rev. B **40**, 4585 (1989); R. J. Birgeneau *et al.*, *ibid.* **39**, 2868 (1989).
[36]J. Akimitsu and Y. Ito, J. Phys. Soc. Jpn. **40**, 1621 (1976).
[37]C. L. Kane *et al.*, Phys. Rev. B **41**, 2653 (1990).